SYSTEMATIC INVERSION OF RECEIVER FUNCTIONS AND SURFACE WAVE DISPERSION FOR CRUSTAL STRUCTURE IN CENTRAL ASIA

Charles J. Ammon[1], Winchelle Sevilla[1], Robert B. Herrmann[2], and George E. Randall[3]

Penn State University[1], Saint Louis University[2], and Los Alamos National Laboratory[3]

Sponsored by National Nuclear Security Administration
Office of Nonproliferation Research and Engineering
Office of Defense Nuclear Nonproliferation

Contract No. DE-FC03-02SF22498[1,2] and W-7405-ENG-36[3]

ABSTRACT

We report on our investigations into the seismic structure of the lithosphere in central Asia using surface waves and receiver functions. We rely on global and regional tomographic analyses for long-period surface wave dispersion constraints on the structure that are supplemented with short-period observations measured directly from regional signals (when available). This paper is an overview of receiver function complexity across the region using results from previous studies and receiver functions from many of the permanent stations. We have completed short-period tomographic imaging of the central and eastern Tibetan Plateau using Love and Rayleigh waves with periods between 10 and 40 seconds. The short period information is critical to tight constraints on shallow shear-wave velocity structure, but the measurements are sensitive to source location and origin time uncertainties. We have also surveyed receiver functions from the INDEPTH III, northeast China, and Tien-Shan Continental Dynamics temporary deployments. We illustrate the combined inversion of surface waves and receiver functions using a variety of model constraints focusing on select stations and provide information to access on-line results (earth models, etc.).

OBJECTIVES

Our objectives are the construction of station-centric shear-velocity profiles for regions surrounding broadband seismic stations throughout central Asia. Application of the technique in the region provides an opportunity to revise models of the crust and upper mantle structure throughout the region and to exploit the global and regional work of previous seismic verification research (e.g. Pasyanos et al., 2001; Ritzwoller & Levshin, 1998, Larson and Ekstrom, 2001, Stevens and McLaughlin, 2001). The resulting shear-velocity models provide a single structure consistent with a range of observations and which can be tested as a tool for the construction of mode isolation filters that can help improve surface wave magnitude estimates. We also plan to explore the possibility of adding additional data to our inversions of receiver functions and surface wave dispersion. The diverse seismic activity throughout the region will facilitate cross-validation of the mode isolation filters with simple empirical filters constructed using larger events with adequate signal-to-noise ratios.

Estimating Subsurface Shear Velocities

Subsurface geology generally has a broad "wavenumber" spectrum containing sharp, or high-wavenumber, changes in velocity near the Earth's major geologic boundaries and smooth low-wavenumber variations in regions of relatively uniform geologic structure. Access to the full spectrum of earth structure requires that we exploit signals that span a wide frequency range and that are sensitive to the entire spectrum of heterogeneity. Surface waves, travel times, and direct-wave amplitudes, for example, are sensitive to smooth variations in earth structure; reflected and converted waves are sensitive to velocity contrasts. Combining seismic data in joint inversions is an obvious approach to improve estimates of earth structure. To successfully combine data in an inversion, we must insure that all the data are sensitive to the same (or related) physical quantities and that they sample or average structure over comparable length scales. Recent advances in surface wave tomography have provided an opportunity to combine localized surface wave dispersion estimates with other data such as P- and S-wave receiver functions. Ammon and Zandt (1993) used surface wave dispersion observations to try and distinguish between competing models of the Mojave desert, but Özalaybey et al., (1997) pioneered a formal, joint inversion of these data. They nicely illustrated the value of even a limited band of dispersion values to help reduce the trade-off between crustal thickness and velocity inherent in receiver function analyses. Specifically, they used Rayleigh wave phase velocities in the 20–25 second period range to help produce stable estimates of crustal thickness in the northern and central Basin & Range. The limited bandwidth did not permit resolution of details in the crust and they limited their inversion (or at least their interpretation) to depths above 40 km. More recent authors have exercised the approach and combined the data with additional a priori model constraints (Du and Foulger, 1999; Julia et al., 2000). Recent accomplishments in global and regional tomography now provide a more complete band of dispersion measurements to combine with receiver functions that allow us to improve the resolution of earlier works.

Surface wave dispersion measurements are sensitive to broad averages, or low wavenumber components of the earth structure. They provide valuable information on the absolute seismic shear velocity but are relatively insensitive to sharp, high-wavenumber velocity changes. Generally surface wave inversions must be constrained using a particular layer parameterization (e.g. near-surface, upper-crust, lower crust, mantle lid, deep mantle), resemble an a priori model, or substantially smoothed to stabilize earth-structure estimation. Despite these drawbacks, surface wave dispersion values contain important constraints on the subsurface structure, and the general increase in depth sensitivity with depth allows an intuitive understanding of their constraints on structure. Additionally, modeling dispersion values facilitates a broadband inversion by reducing the dominance of Airy phases, which pose problems when constructing broadband misfit norms to model seismograms directly. Perhaps most important for our application is the ability to localize Earth's dispersion properties using seismic tomography. The idea is now well established and global dispersion models exist for a broad range of frequencies (e.g. Larson and Ekström, 2001; Stevens et al., 2001). The localization of dispersion allows us to isolate the variations in properties spatially and global models of surface wave dispersion exist and are readily available for application to other studies such as the proposed work.

Receiver functions are time series computed from three-component body-wave seismograms that show the relative response of the Earth structure near the receiver (e.g. Langston, 1979). Source, near-source structure, and mantle propagation effects are removed from the seismograms using a deconvolution that sacrifices P-wave information for the isolation of near-receiver effects (Langston, 1979; Owens et al., 1984; Ammon, 1991; Cassidy, 1992). Receiver function waveforms are a composite of P-to-S (or S-to-P) converted waves that reverberate within the structure near the seismometer. Modeling the amplitude and timing of those reverberating waves can supply valuable constraints on the underlying geology. In general, the receiver functions sample the structure over a range of ten's of kilometers from the station in the direction of wave approach (the specific sample width depends on the depth of the deepest contrast). Stations sited near geologic boundaries can produce different responses for different directions. Recent innovations in receiver function analysis include more detailed modeling of receiver function arrivals from sedimentary basin structures (e.g. Clitheroe et al., 2000), anisotropic structures (e.g. Levin and Park, 1997; Savage 1998), estimation of Poisson's ratio (e.g., Zandt et al., 1995; Zandt and Ammon, 1995; Zhu and Kanamori, 2000, Ligorría, 2000), reflection-like processing of array receiver functions (e.g., Chevrot and Girardin, 2000; Ryberg and Weber, 2000) and joint inversions (e.g., Özalaybey et al., 1997; Du and Foulger, 1999; Julia et al., 2000).

Our joint inversion method is similar to that of Özalaybey et al. (1997) except that we use jumping, smoothness, and constraints to include as much *a priori* information into the inversion as is available. We combine the receiver function and surface wave observations into a single algebraic equation and account for their different physical units and equalize their importance in the misfit norm by weighting each data set by an estimate of the uncertainty in the observations and the number of data. We also append smoothness constraints and *a priori* model constraints on the deepest part of the model. Although we cannot resolve fine details in the deep upper mantle, these regions can impact our results since surface wave dispersion values at intermediate and longer periods are somewhat sensitive to this deeper structure. We believe that it is important to have a reasonable basement structure so that our results are more consistent with global models. We extend our models to about 500–700 *km* to insure this consistency. The resulting inversion equations are

$$\begin{bmatrix} \sqrt{\frac{\mathbf{p}}{\mathbf{w}_s^2}}\mathbf{D}_s \\ \sqrt{\frac{\mathbf{q}}{\mathbf{w}_r^2}}\mathbf{D}_r \\ \sigma\Delta \\ \mathbf{W} \end{bmatrix} \cdot \mathbf{m}_{i+1} = \begin{bmatrix} \sqrt{\frac{\mathbf{p}}{\mathbf{w}_s^2}}\mathbf{r}_s \\ \sqrt{\frac{\mathbf{q}}{\mathbf{w}_r^2}}\mathbf{r}_r \\ 0 \\ 0 \end{bmatrix} + \begin{bmatrix} \sqrt{\frac{\mathbf{p}}{\mathbf{w}_s^2}}\mathbf{D}_s \\ \sqrt{\frac{\mathbf{q}}{\mathbf{w}_r^2}}\mathbf{D}_r \\ 0 \\ 0 \end{bmatrix} \cdot \mathbf{m}_i + \begin{bmatrix} 0 \\ 0 \\ 0 \\ \mathbf{W} \end{bmatrix} \cdot \mathbf{m}_a \qquad (1)$$

where $\mathbf{p}$, $\mathbf{q} = 1 - \mathbf{p}$, σ, and $\mathbf{W}$ are weights that control the relative importance of receiver functions, dispersion values, smoothness, and *a priori* model constraints in the norm minimized during the inversion. The data comprise the vectors $\mathbf{r}_s$ and $\mathbf{r}_r$, and the partial derivatives fill the matrices $\mathbf{D}_r$ and $\mathbf{Ds}$. The matrix Δ is a finite-difference stencil that "computes" model roughness, and the matrix $\mathbf{W}$ is a layer-dependent weight that is used to insure the model blends smoothly into the *a priori* model, $\mathbf{m}_a$, at depth. The values of $\mathbf{w}_s$ and $\mathbf{w}_r$ are equal to the product of the number of points in the dispersion curve and receiver functions and the variance of the observations. The second term on the right is added to create the "jumping" inversion scheme (e.g. Constable et al., 1987; Ammon et al., 1990) and allows us to solve for (and constrain) the shear-velocity models as opposed to shear-velocity correction vectors. Equation (1) is solved in a least-squares sense for the model, $\mathbf{m}_{i+1}$, starting with an initial model $\mathbf{m}_0$. The procedure generally converges in a few iterations.

Estimating Receiver Functions

When the data are high-quality and the receiver structure is not too complex, the choice of a deconvolution procedure does not make much difference. However, when the noise in the seismograms is substantial, or the receiver structure is complex, different deconvolution approaches have strengths and weaknesses. We will compute receiver functions using the iterative time-domain deconvolution procedure described by Ligorría and Ammon (1999). We prefer the iterative approach, which is based on the Kikuchi and Kanamori (1982) source-time function estimation algorithm, for several reasons. First, in the iterative approach the receiver function is constructed by a sum of Gaussian pulses which produces a flat spectrum at the longest periods. The flat long-period spectrum can be viewed as *a priori* information that helps reduce side-lobes that may result of spectral or singular-value truncation stabilization procedures. The reduction of side-lobes eases the interpretation and helps stabilize "low-frequency" receiver functions. Second, the iterative approach constructs a causal receiver function, which is what we expect in all cases of reasonable earth structure. This is a subtle difference from spectral techniques (e.g. Langston, 1979; Park and Levin, 2000) which can

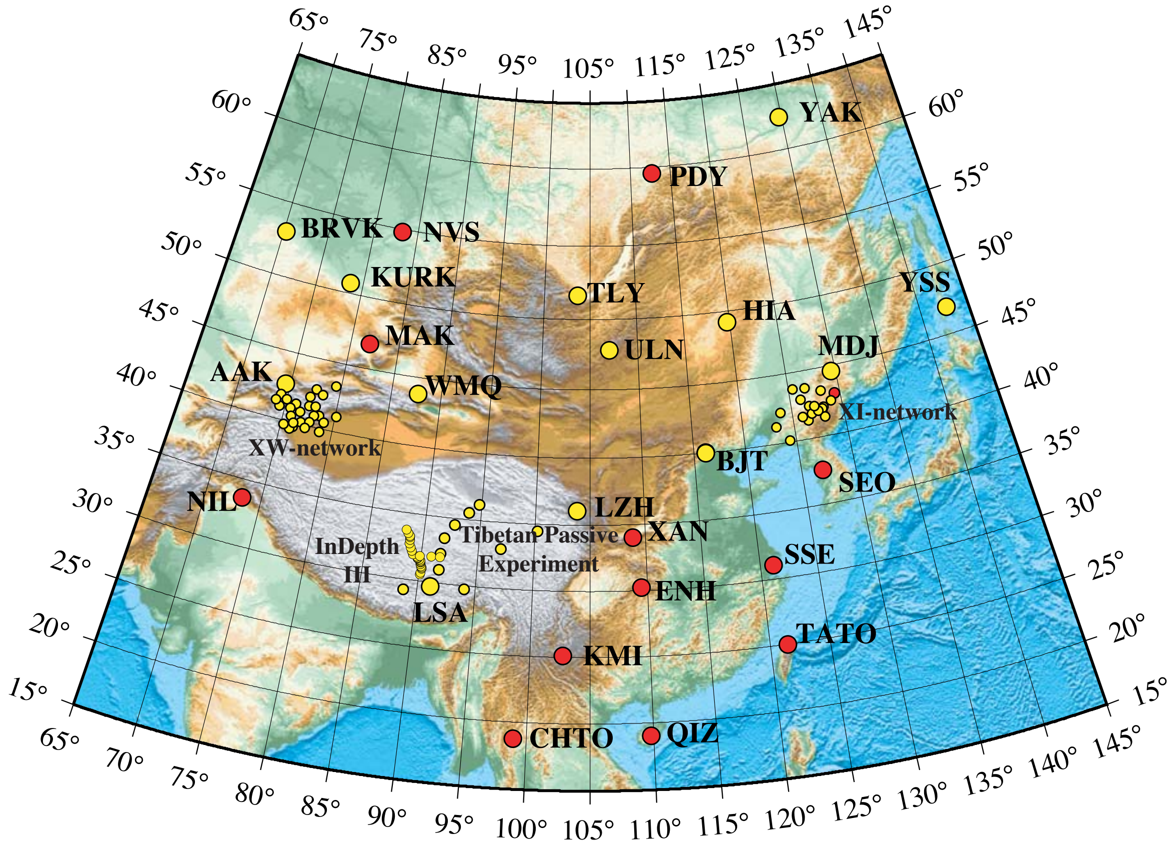

Figure 1. Location of stations that we have analyzed so far in this project. Large and small circles represent GSN and the temporary network stations respectively. Yellow symbols identify stations for which we have computed receiver functions (and performed Poisson's Ratio analyses). Stations currently being processed are identified by red symbols.

always introduce a component to the signal before the P-wave. The acausal component of the spectral signal may be small, but still important to the satisfaction of the convolutional model that defines a receiver function, i.e.,

$$\mathbf{R}(\mathbf{t}) = \mathbf{Z}(\mathbf{t}) * \mathbf{E}_{\mathbf{R}}(\mathbf{t}) . \qquad (2)$$

In equation (2), $\mathbf{R}(\mathbf{t})$ and $\mathbf{Z}(\mathbf{t})$ are the radial and vertical seismograms, and $\mathbf{E}_{\mathbf{R}}(\mathbf{t})$ is the radial receiver function (a similar equation holds for the transverse component). The point is that even when the receiver function estimation is unstable, spectral deconvolutions may satisfy (2) quite well. The iterative time-domain approach, which can be restricted to produce the best *causal* solution, may not always satisfy (2). Experienced modelers have always been able to identify failed receiver functions, but the misfit to (2) available from iterative deconvolutions provides quantitative information that can be used when stacking signals, or in extreme cases, to discard obviously failed deconvolutions. In our case we find using a threshold cut-off of 80-90% of the radial power fit allows us to quickly discard poorly constrained deconvolution results, enabling an efficient and objective select of the data to include in further analysis.

RESEARCH ACCOMPLISHED

Receiver Function Computation

We have processed 13 of the 26 GSN stations and 44 stations from temporary networks in central and eastern Asia, which includes 18 stations from the XI-network and 26 stations from the XW-network shown in Figure 1. Computation of the receiver functions follows a simple approach by gathering first teleseismic P-waveforms of events greater

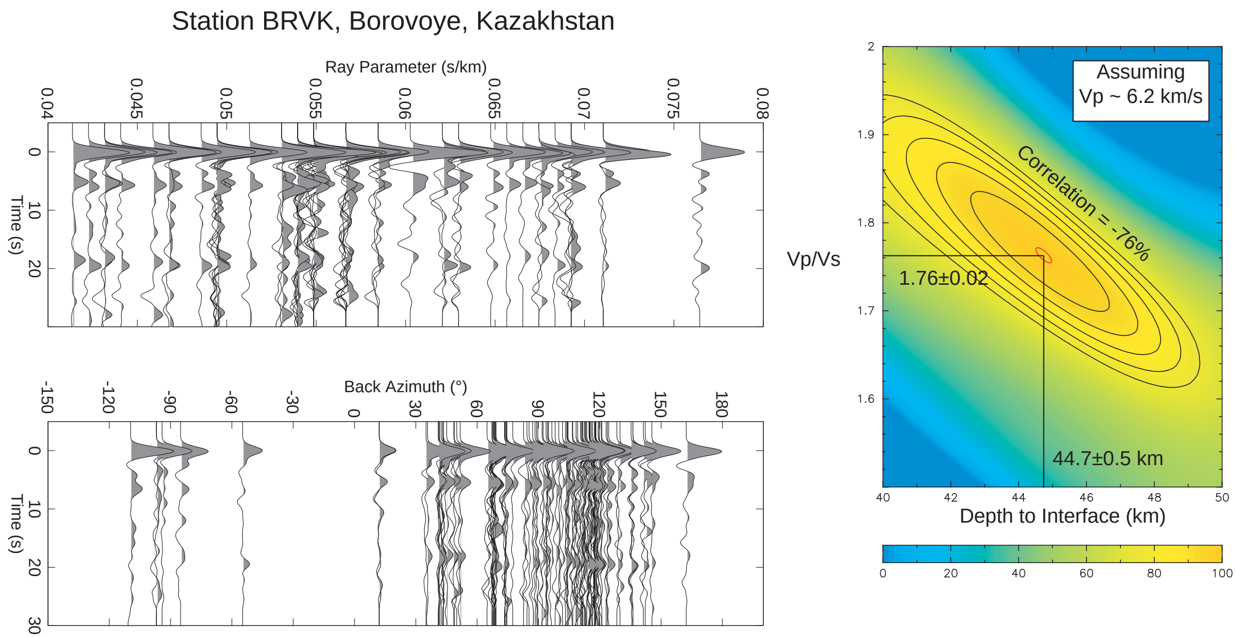

Figure 2. Sample receiver function observations and a limited analysis of Poisson's ratio and crustal thickness (assuming Vp ~ 6.2 km/s). The observed receiver functions are shown as a function of ray parameters (sin of the P-wave incident angle) and as a function of back azimuth. The data do not sample the azimuthal structure uniformly as teleseisms are predominantly observed from western-Pacific subduction zones. The ray parameter sampling is good, and identifiable conversions and multiples are seen clearly for a range of incident angles. The image on the right shows the results of stacking all waveforms to identify the crust-mantle transition. Uncertainties were estimated using a jack-knifing technique. These uncertainties are conservative since they also depend on the assumed P-velocity of the crust. As a result of azimuthal sampling, the results are most reflective of the structure to the east of the station.

than Mw 5.5 for a given station. Then, we use the iterative time-domain deconvolution of Ligorria and Ammon (1999) to do the computation and select the best receiver functions for analysis. We cluster the receiver functions as a function of back azimuth and ray parameter (the amount of data determines the feasibility of this approach). Our analysis usually begins with a relatively simple stacking procedure that allows the estimation of the Vp/Vs ratio (or Poisson's ratio) and crustal thickness (Zhu and Kanamori, 2000). The analysis produces relatively good estimates when the simple assumptions (relatively flat crust-mantle boundary) are satisfied. Then the radial receiver functions are combined with the surface wave dispersions for joint shear-velocity inversions. As had been mentioned earlier, the receiver functions may exhibit different patterns as a function of back azimuths such that we assigned a narrow range of back azimuths to be used in the inversions. The simplicity and the similarity in the forms of the receiver functions primarily dictate the criteria we used for the bounds. After choosing the bounds, we stacked the receiver functions and use this stack for the joint inversions.

An Example Analysis, Station BRVK, Borovoye, Kazakhstan

Example receiver functions for station BRVK in central Asia are shown in Figure 2. BRVK is a station of IRIS/IDA - GSN network located at coordinates 53.05810 N and 70.28280 E and is situated on top of a granitic pluton (Richards et al., 1992). Seismograms recorded at this station are high quality because of the very low microseisms on the site (e.g. Kim et al., 1993; Kim and Ekstrom, 1996) making it a well suited for a receiver function analysis. Previous receiver function studies of BRVK (Kim et al., 1993) estimated a 45 km thick crust along the direction 87° from north. Since the receiver functions vary with azimuth and ray parameter we summarize our observations in two profiles, one for azimuth and one for ray parameter. As a first order approximation of the structure, we've ignored azimuthal variation and performed a stacking procedure to use the waveforms to estimate the thickness and Poisson's ratio of the crust (assuming that Vp ~ 6.2 km/s) using the method of Zhu and Kanamori (2000). The resulting fits are reasonable, with a thickness value of about 45 km and a Poisson's ratio of 0.26. We will perform similar analyses and inversions for each station with suitable data.

We show the results of an example joint inversion in Figure 3. The receiver functions are shown at the upper left panel, and correspond to averages from five events with similar ray parameter and back azimuth. The lower left panel shows the group velocities, which are from the Pasyanos et al. (2001) surface wave group velocity model. The panels along the right show the initial and estimated velocity profiles in a direction roughly east of the station. The fit to both receiver functions and surface wave dispersion curves in Figure 3 is very good, which may reflect the simplicity of the crustal structure underlying the station. The resulting shear-velocity model is quite simple, with a PREM-like mantle and the crustal thickness and poisson's ratio that you would expect in a platform (Zandt and Ammon, 1995). The only unusual feature is low shear-velocity zone between 20 and 30 km depth (~10% slower than the "typical" continental crust used at the top of the initial model). This zone corresponds to the prominent trough at around three seconds on the stacked receiver functions. The crust-mantle transition is relatively sharp, indicated by the strong converted phases at around 18 seconds on both stacks, which is consistent with previous observations (Kim et al., 1993). The crustal thickness is about 48 km for the joint inversion result.

Bulk Crustal Structure Comparisons

We plot the crustal thicknesses of our results together with the estimated thickness under the Tibetan passive-source experiment (Mejia, 2001) and INDEPTH III experiment (Diehl, 2003) with the Crust 2.0 model (global crustal model at 2x2 degrees) of Bassin et al. (2000) (Figure 4). We don't accept the values of Crust 2.0 in all places, but it is a useful reference for comparison. The results show good agreement; the mean difference between the our results and Crust 2.0 is less than one *km*, the standard deviation of the differences is between 5 and 6 *km*. Median crustal thicknesses for the XI- and XW-networks (eastern and central Asia, respectively) are 32 *km* and 53 *km*. We also examined variations of the bulk crustal *Vp/Vs* ratio and show them as a function of crustal thickness (Figure 4). The plot can help us to identify which stations produce *Vp/Vs* values that plot outside the *Vp/Vs* bounds appropriate for the crustal materials. These unrealistic values are a result of crustal complexity which is not included in the simple *Vp/Vs* ratio estimation procedure.

CONCLUSIONS AND RECOMMENDATIONS

The future thrust of this project is to finish computing the receiver functions of the remaining stations and complete the joint inversion processes to estimate the shear velocity structure beneath all available broadband three-component seismic stations in central Asia. The next year will also include assessment of the potential applications of the velocity models to seismic waveform modeling and seismic event location.

ACKNOWLEDGEMENTS

We thank P. Wessel and W. H. F. Smith, the authors of GMT, for producing easy-to-use, quality software for making maps and charts.

REFERENCES

Ammon, C.J., G.E. Randall, and G. Zandt (1990), On the non-uniqueness of receiver function inversions, *J. Geophys. Res.*, 95, 15303-15318.

Ammon, C.J. (1991), The isolation of receiver effects from teleseismic P waveforms, *Bull. Seism. Soc. Am.*, 81, 2504-2510.

Ammon, C. J., and G. Zandt (1993), The receiver structure beneath the southern Mojave Block, *Bull. Seism. Soc. Am.*, 83, 737-755.

Bassin, C., Laske, G., and G. Masters (2000), The current limits of resolution for Surface Wave Tomography in North America, *EOS Trans AGU*, 81, F897.

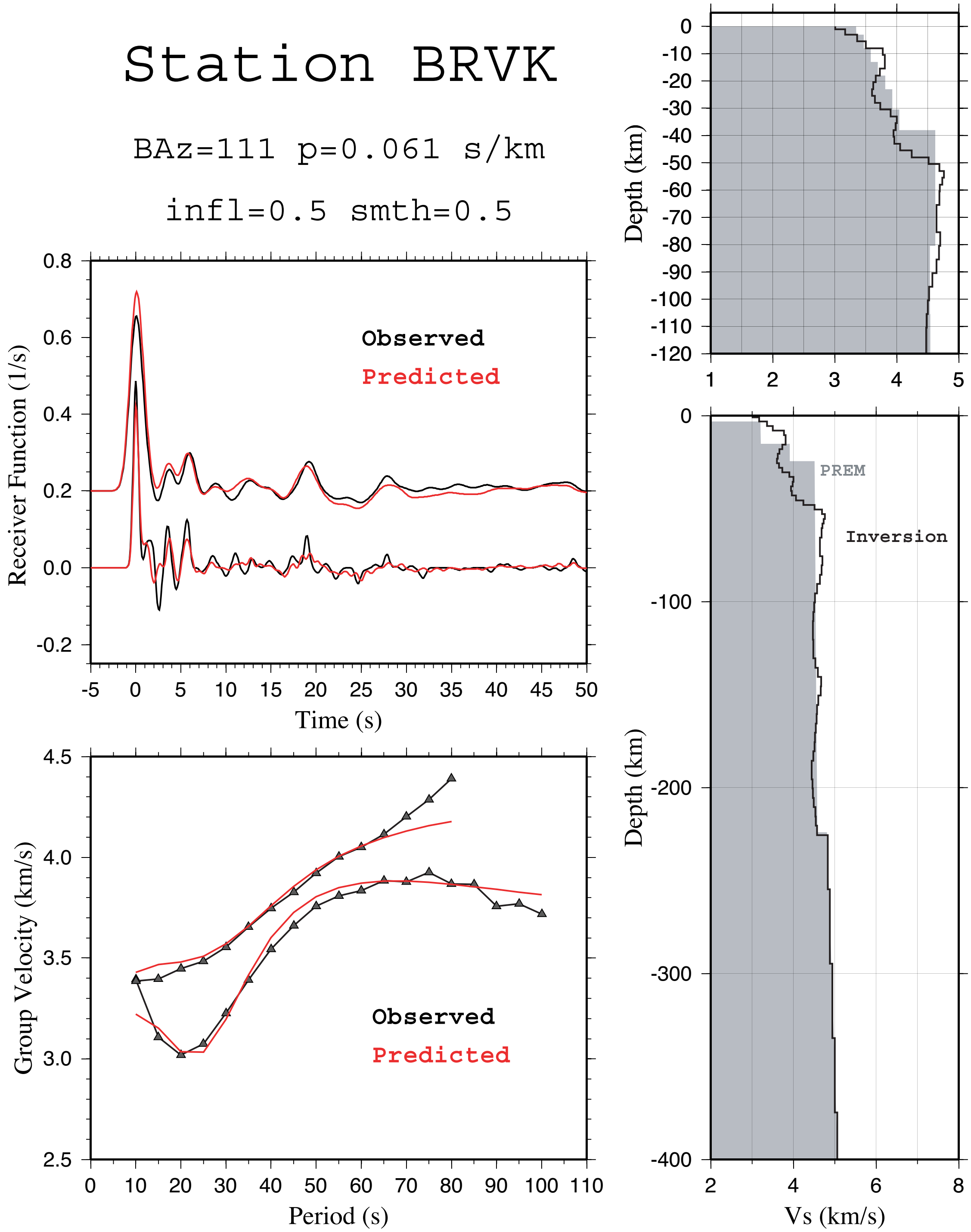

Figure 3. Simultaneous inversion results for the station BRVK using Pasyanos et al., (2001) surface wave dispersion model (lower left panel) and stacked receiver functions (upper left panel) that sample the structure roughly east of the station. A Gaussian width factors of 1.0 (top stacked) and 2.5 (bottom stacked) were used to generate the receiver functions. BAz is the average back azimuth and p is the average ray parameter of the incoming P-waves. The influence parameter, “infl”, balances the weight between the receiver functions and dispersion during the inversion. “smth” is the smoothness weight. On the right panels are the initial model (a modified version of PREM) (shaded in gray) and the estimated shear-wave velocity models.

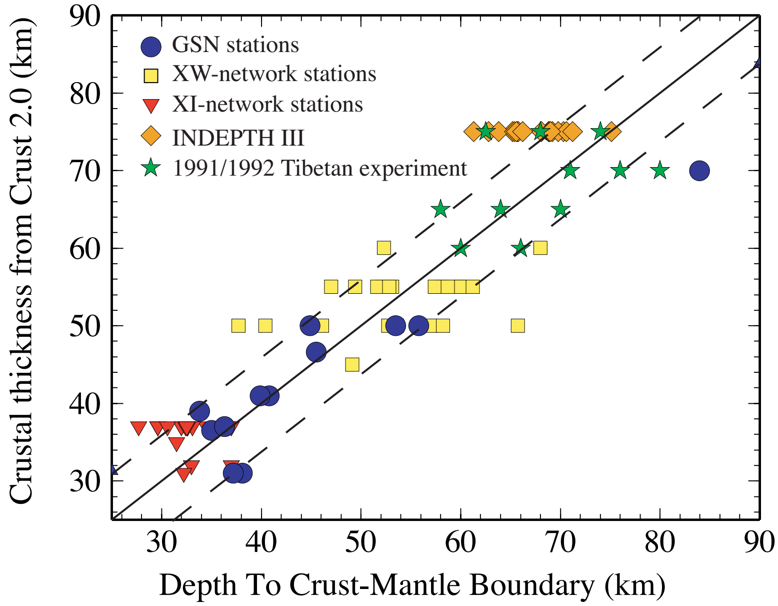

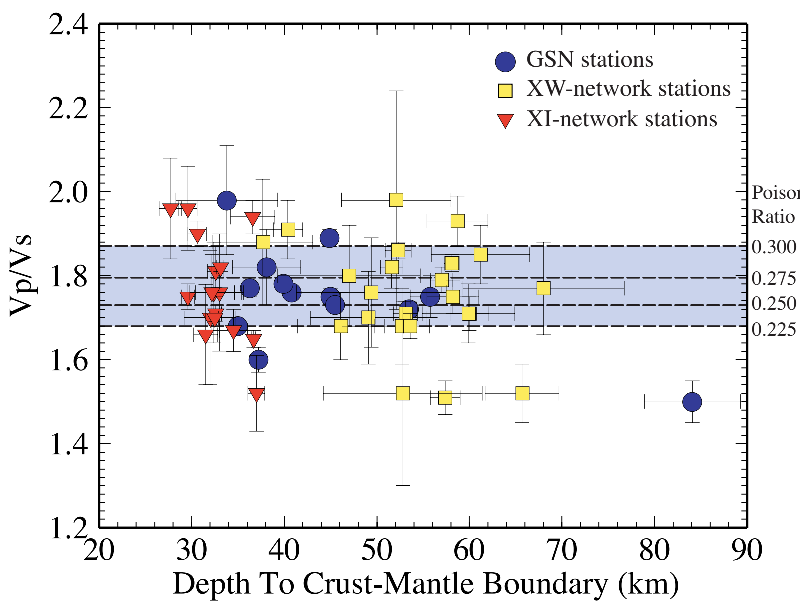

Figure 4. (Top) Plot showing the correlation between the crustal thickness obtained by this study (horizontal axis) and the Crust 2.0 model. Different symbols represent different networks, but all data have been processes the same way. GSN stations generally have much larger data sets than the temporary networks. The dashed lines represent ±1 standard deviation in the model differences. (Bottom) Estimated Vp/Vs ratio variation with crustal thickness. The error bars are uncertainties on the results from the bootstrap method of Julia and Mejia (2004). Dashed horizontal lines are Poison's ratio used as a reference for determining which station is underlain by complicated crustal structure, which are characterized by having a very high or very low

Cassidy, J.F., Numerical experiments in broadband receiver function analysis, *Bull. Seismol. Soc. Am.*, 82, 1453-1474, 1992.

Chevrot, S., and N. Girardin (2000), On the detection and identification of converted and reflected phases from receiver functions, *Geophys. J. Int.*, 141 (3), 801-808.

Clitheroe, G., O. Gudmundsson, and B.L.N. Kennett (2000), Sedimentary and upper crustal structure of Australia from receiver functions, *Australian Journal of Earth Sciences*, 47 (2), 209-216.

Diehl, T. M., Determining crustal Structure Beneath the Tibetan Plateau Using Receiver Functions, *B. S. Thesis*, Penn State University, University Park, PA, 2003.

Du, Z.J. and G.R. Foulger (1999), The crustal structure beneath the northwest fjords, Iceland, from receiver functions and surface waves, *Geophys. J. Int.*, 139, 419-432.

Herrmann, R. B., *Computer Programs in Seismology, 1995*, Saint Louis University, St. Louis, MO, USA.

Jackson, D.D., Interpretation of inaccurate, insufficient, and inconsistent data (1972), *Geophys. J. R. Astron. Soc.*, 28, 97-109.

Julia, J., C. J. Ammon, R. B. Herrmann, and A. M. Correig (2000), Joint Inversion of receiver function and surface-wave dispersion observations, *Geophys. J. Int.* 143, 99-112.

Julia, J., and J. Mejia (2004), Thickness and Vp/Vs ratio variations in the Iberian crust, *Geophys. J. Int.*, 156, 59-72.

Kim, W. Y., and G. Ekstrom, (1996) Instrument responses of digital seismographs at Borovoye, Kazakhstan, by inversion of transient calibration pulses, *Bull. Seism. Soc. Am.*, 86, 191-203.

Kim, W. Y., L. Gao, and P. Richards, (1993) Crust and upper mantle seismic velocity structure beneath Borovoye Observatory, northern Kazakhstan, EOS, Trans., AGU, 74, Suppl., 433.

Kind, R., J. Yuan, J. Saul, D. Nelson, S.V. Sobolev, J. Mechie, W. Zhao, G. Kosarev, J. Ni, U. Achauer, and M. Jiang, Seismic Images of Crust and Upper Mantle Beneath Tibet: Evidence for Eurasian Plate Subduction, *Science*, 298, 1219-1221, 2002.

Langston, C.A. (1979), Structure under Mount Rainier, Washington, inferred from teleseismic body waves, *J. Geophys. Res.*, 84, 4749-4762.

Larson, E. W. F. and G. Ekström (2001), Global Models of Group Velocity, *Pure and Applied Geophys.*, 158, 1377-1399.

Last, R. J., A. A. Nyblade, C. A. Langston and T. J. Owens (1997), Crustal structure of the East African Plateau from receiver functions and Rayleigh wave phase velocities, *J. Geophys. Res.*, 102, 24,469-24,483.

Levin, V., and J. Park (1997), Crustal anisotropy in the Ural Mountains from teleseismic receiver functions, *Geophysical Research Letters*, 24 (11), 1283-1286.

Ligorria, J.P., and C.J. Ammon, Iterative deconvolution of teleseismic seismograms and receiver function estimation, *Bull. Seism. Soc. Am.*, 89, 1395-1400, 1999.

Mejia, J. (2001), Lithospheric structure beneath the Tibetan Plateau using simultaneous inversion of surface wave dispersion and receiver function, *Ph.D. thesis, St. Louis University.*

Owens, T.J., G. Zandt, and S.R. Taylor (1984), Seismic evidence for an ancient rift beneath the Cumberland Plateau, Tennessee: A detailed analysis of broadband teleseismic P waveforms, *J. Geophys. Res.*, 89, 7783-7795.

Özalaybey, S., M.K. Savage, A.F. Sheehan, J.N. Louie, and J.N. Brune (1997), Shear-wave velocity structure in the northern Basin and Range Province from the combined analysis of receiver functions and surface waves, *Bull. Seismol. Soc. Am.*, 87, 183-199.

Pasyanos, M.E., W.R. Walter, and S.E. Hazler (2001), A Surface wave dispersion study of the Middle East and North Africa for Monitoring the Comprehensive Nuclear-Test-Ban Treaty, *Pure and Applied Geophys*, 158, 1445-1474.

Randall, G. E. (1989), Efficient calculation of differential seismograms for lithospheric receiver functions, *Geophys. J. Int.*, 99, 469-481.

Richards, P., K. Won-Young, and G. Ekström (1992), Borovoye Geophysical Observatory, Kazakhstan, *EOS Trans AGU*, 73, 201--206.

Ritzwoller, M. H. and A. L. Levshin (1998), Eurasian surface wave tomography: Group velocities, *J. Geophys. Res., 103*, 1839-1878.

Ryberg, T., and M. Weber (2000), Receiver function arrays; a reflection seismic approach, *Geophys. J. Int.*, 141 (1), 1-11.

Savage, M.K. (1998), Lower crustal anisotropy or dipping boundaries? Effects on receiver functions and a case study in New Zealand, *J. Geophys. Res.*, 103 (7), 15,069-15,087, 1998.

Stevens, J. L. and K. L. McLaughlin (2001), Optimization of Surface Wave Identification and Measurement, *Pure and Applied Geophys*., 158, 1547-1582

Zandt, G., and C. J. Ammon (1995), Continental Crustal composition constrained by measurements of crustal Poisson's ratio, *Nature*, 374, 152-154.

Zandt, G., S.C. Myers, and T.C. Wallace (1995), Crust and mantle structure across the Basin and Range-Colorado Plateau boundary at 37 degrees N latitude and implications for Cenozoic extensional mechanism, *J. Geophys. Res.*, 100 (6), 10,529-10,548.

Zhu, L., and H. Kanamori (2000), Moho depth variation in Southern California from teleseismic receiver functions, *J. Geophys. Res.*, 105 (2), 2969-2980.